A novel method for application of non-conventional sources of energy with power quality improvement for local non-linear load using MLMS

T Kishore Kumar, Dr. P. Balachennaiah, P. Durga Prasad, Dr. C. Kumar Reddy

Address: Department of Electrical and Electronics Engineering, KSRM College of Engineering, kadapa, AP, India.,
Dept of Electrical and Electronics Engineering, AITS, Rajampet, AP, India.

Email:

Abstract

In an Energy Micro-Grid, a collection of energy networks is used to meet all of the local area's energy needs. The use of energy storage systems (e.g., electrochemical storage) appears to be a promising solution, taking into account costs, supply security, technological maturity, and ease of installation. It uses a micro-grid to integrate wind and solar photovoltaic electricity (PV) sources with energy storage batteries to feed the non-linear load (BES). The switching controls and the adjustment of the grids all address power quality (PQ), power reliability, non-linear load correction and economical resource usage. In order to adjust for nonlinear load and improve the PQ system a modified version for Adaptive Filtering Technology is employed, including the "momentum-based least mean square (MLMS)" technology, giving GVSC control signals. As a result, the convergence rate is improved, and the limitations of conventional control of the same family are removed. Back electromotive force control technique is used to obtain switching signals from conventional vector control scheme and encoder less estimation of speed and Wind turbine-powered SG rotor position. Using perturb and observe (P&O) maximum power point estimation for wind and adaptive P&O with variable perturbation step size for solar MPP estimation, the external environmental unrest can be overcome. Under steady state and dynamic conditions, including changing wind speeds, intermittent solar isolation, and variable load conditions, MATLAB/SIMULINK simulation results are obtained.

Keywords: Power quality, MLMS, Power generation, Solar PV, Wind energy, Maximum power point and perturb and observe.

1. INTRODUCTION

Natural sources of energy that have virtually no pollution or renewable energy sources must be taken into consideration. Wind energy is one of the renewable energy sources that ensures clean energy since wind energy generators for conversion of electricity may be efficiently gathered and used. Clean energy solution is photovoltaic control. Furthermore, it can be used without the usage of a rotary generator. The more wind power managed by PV, which goes hand in hand, should contribute to some extent, because strong winds generally occur at night and on cloudy days [1].

As a result of an efficiently and cost-effective use of renewable energy sources [2], some energy sources, such as wind turbines and solar panels, are incorporated. As the performance of these systems depends on wind speed and solar irradiation, its reliability is under all conditions reduced in meeting load needs. Some researchers have suggested combining diesel generators with wind/solar energy system [3][4]. Micro-grids commonly integrate these energy sources as power generators for distribution via appropriate power conversion stages. For example, DC-DC-AC converters are used by solar photovoltaic generators, and AC-DC-AC converters with local control are used by generators of wind [5].

When the wind speed falls below the cut-in speed, the wind generator is turned on. The wind generator starts to generate with unregulated frequency when wind speeds resume, until it is linked to the micro-grid and operates through a loop control. The absence of the wind generator means that the battery power generation can maintain crucial charges dependent on the battery charge. In those queries about grid connection and insulation a wind/PV house power system powered by the EV battery will be provided. A bidirectional converter is primarily controlled by a concurrent inverter [6] to operate a wind generator, interfacing with the back-to-back AC-DC-AC and the Battery interface.

It is currently actively supported to create the public LV network-connected PV system. These systems are usually from several to ten kWP in size, and on the top of dwellings or public buildings are solar panels installed. The efficient photovoltaic system operation varies, including sun intensity, cell temperature and cloud shading. The time unpredictability of production of electrical energy leads to expected power quality issues such as voltage imbalances, flushes, and downsizing [7].

The PV system is connected to the grid by a power converter and an inverter for modulation of pulses width. These interface converters provide a range of functions, including PV output adjustments to meet inverter voltage and maximum power point tracking, to operate the PV system as efficiently as feasible. There is a risk that converters will introduce harmonic distortions at both lower and higher frequency rates which result in parallel and series resonances, condenser bank and transformer overheating and the misuse of protective devices that could create problems of power quality [8]. When electricity prizes and demand are at their highest level, they try to feed the most power they can. The system thus succeeded

in recovering its excess revenues. When the SECS and the WEGS (Windows Systems) combine, the system's efficiency and reliability will be improved [9][10]. The voltage and frequency of electric WEGS compliance generated to meet grid code can be controlled and controlled [11], VSCs are adapted as an interface between the machine and the utility grid as the full voltage converter. [12]. For example, 10 voltage stresses caused by harmonic current have been shown to increase the operating temperature of a power bank by 7 and can reduce the expected lifetime of the bank by 30. [13]. Because of its inherent simplicity and strength, the least mean square (LMS) algorithm [14],[15] has become one of the most popular adaptive filter algorithms. But LMS is often slowly converging. Several LMS changes have been proposed over the year to remedy this situation. One of those changes is Proaki's first proposed LMS (MLMS) adaptive algorithm [16]. Roy and Shynk [17] have shown that the MLMS approximates the conjugate algorithm of gradients. MLMS is helpful when error bursting is problematic in applications. The MLMS recursion is WK+1= WK+μ(DK-WTK) XK+α(WK-WK-1) the parameter estimate at the kth iteration, DK is a real valued desired response XK = [x1k , x2k , ……, xdk]T Ɛ Rd is the input response, α Ɛ (-1.1) is the momentum factor, and μ >0 is the input size.

The approximations of the conjugate gradient algorithm (MLMS) are being used for the improvement of the energy quality of the gird-connected wind-based solar system [18]. It overcomes the slow convergences restricts of the convectional LMS and provides advantages when error bursting is the problem in applications. Compared to LMS, MLMS eliminates weight convergence dependence on step size, while it provides higher performance with high-noise signal. The improved dynamic performance comes from inclusion of feed terms for changes in wind and solar insolation. Identification if it is possible to achieve maximum output by using maximum output (MPP) systems for extracting both resources. A literature listing specifically from convection schemes (p &o), incremental conductance (InC), computer soft logic, artificial network neural, and optimization-based schemes [19–21] offers a variety of techniques. In this literature there is a special listing. The non-linear charge presence leads to additional problems in the power quality, including waveform voltage and current distortion. Finally, an important issue to be investigated may be the interaction between the harmonic currents and loads of the inverters; a harmonic distortion which can be multiplied by the resonant behaviour of the grid [21].

2. SYSTEM CONFIGURATION

Figure.2.1 depicts the AC micro-grid system with wind and solar panels in which two VSCs, MVSC and GVSC, back-to-back, provide decoupling power control. The DC connection via the BES and bidirectional DC-DC converters is connected to a solar PV array (one-stage). The combined wind turbine-driven SG and solar photovoltaic generation meet the demand for load. At a point of common linkage, the nonlinear load is connected (PCI). The grid includes the excess PV array and

wind power generation. The harmonics are filtered via a PCI connected ripple filter. The interface inductors are linked with GVSC in series to reduce the current harmonics. The DC engine simulates the wind emulator. With solar insolation change, the variable wind speeds, sudden charge disconnect, the promising system performance is achieved.

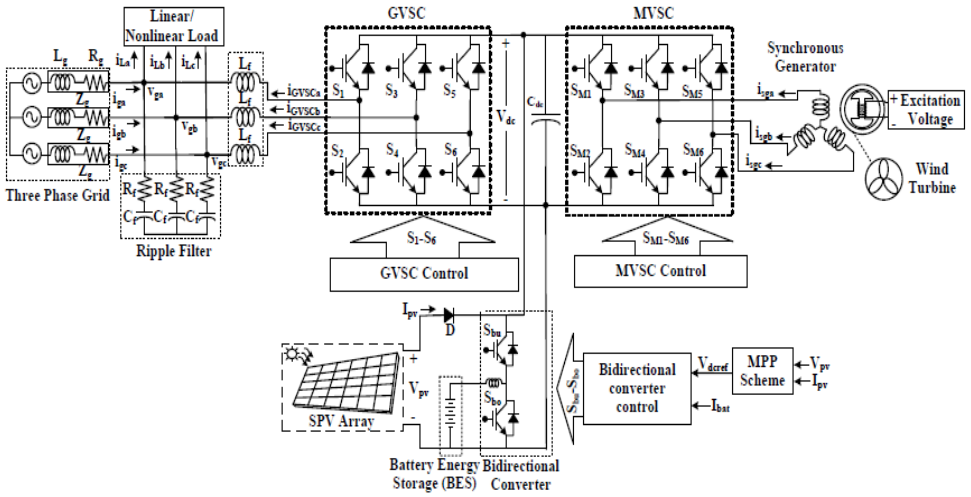

Figure 2.1. System configuration.

The proposed system control algorithms comprise three sub-sections. The GVSC switching controller is based on MLMS, Vector Control (VC) and Bidirectional Conversion Control is based on Vector Control (VC). The GVSC switching control is based upon MLMS (VC). Together with MPP approaches, these control algorithms for wind and solar assess the efficiency of the system.

A. MPP Extraction Scheme

Inherently, solar insolation and wind speed vary with time and place. On the other hand, the system using those 2 renewables requires the best energy extraction approach to be applied individually. The P&O control system follows the wind MPP effectively while adaptive P&Os are used to estimate solar MPP with variable disturbance step size.

Wind-P&O Control Scheme

The P&O scheme is the most common and easily controlled way to identify the MPP from non-linear wind characteristics. This algorithm controls the speed of the wind turbine generator (gene set.) to achieve the MPP; (Pwind). The SG speed is disturbed in the given direction while observing the force drawn from the SG. When the SG's power increases, it signifies that the SG gets stronger. The velocity of the SG must therefore be disrupted in the same way that the optimum operating point has gone toward the MPP. On the other hand, if the SG power decreases, the

optimal operating point will be moved away from the MPP, and the disruptive SG speed will need to be reversed now.

Solar-Adaptive P&O MPP Control

MPP approaches with a fixed disturbance are likely to oscillate. The control calculates the MPP operating point with a short circuit current product with an ideal constant proportionality. The perturbation step size tuning procedure is carried out based on irradiance level and operating point oscillations. This led to the naming of rough and fine tuning. The solar photovoltaic array controls the level of insolation of coarse tuning and its oscillation around the MPP determines fine tuning.
The widespread equation as,
$V=V(n)+sign\{V(n)-V(n-1)\}*sign(\Delta P)*\Delta V(n)$
In this case, the sign (•) sets +1 or -1 according to the value within the function. This control effectively traces the MPP under sudden changes in the level of insolation and reduces oscillations around the MPP by disturbing the step size.

B. GVSC Switching Control

The control system for the GVSC is presented in Figure.2.2. Use of MLMS-based adaptive control enables power-quality improvement and load-current distortion compensation in a time-invariant system with stochastic inputs like variable wind and solar conditions. This device is supplied with the GVSC switching pulses. This is the case when the least square algorithm progresses. MLMS can be easily managed for system conditions and parameter uncertainty. Adding "momentum" enables quicker convergence. It updates the weight according to the previous gradient without affecting the complexity of the system. This accelerates the convergence process and effectively compensates the load harmonics with noise-polluted inputs.

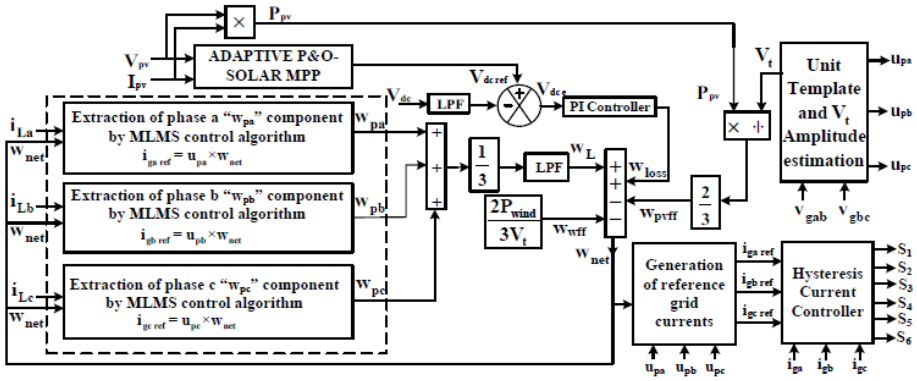

Figure 2.2. Control structure for GVSC.

MLMS Algorithm

The scheme of the MLMS algorithm is shown in Figure.2.3. LMS with previous weight vectors is updated to achieve the next weight vector. MLMS's second order update weight equation is as follows,

$$w(n+1) = w(n) + 2\xi e(n)x(n) + \alpha[w(n) - w(n-1)]$$

where, ξ is the step size controlling the convergence rate, α is the momentum factor that scales the gradient descent, and the working ranges are ξ>0 and α<0.

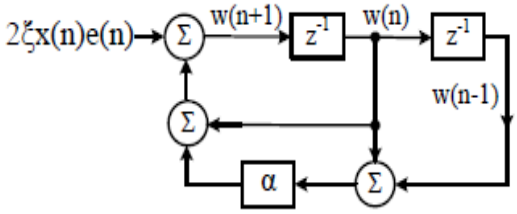

Figure 2.3. MLMS algorithm.

The derivation of the second order weight update equation of MLMS, is given as follows. The variables used are given as,

w(n) is the weight vector $= [w_0(n), w_1(n), \ldots., w_{M-1}(n)]^T$

e(n) is the output error $= d(n) - w^T(n)x(n)$

x(n) is the input signal $= [x(n), \ldots., x(n-M+1)]^T$

d(n) is the desired response and y(n) is the analogous estimate of d(n) and is given as,

$$y(n) = w^T(n)x(n)$$

The MLMS is the recursion of the weight increments and can be derived from the simplified implementation of conjugate gradient algorithm.

C. MVSC Switching Control

Figure 2.4 illustrates how to implement the MVSC control. The control system controls both the current direct reference axis (Id ref) generator and the quadrature-axis (Iq ref). The torque-producing component comprises two components: the square axis and torque-products. The wind-P&O MPP Scheme employs the benchmark generator speed to compare the SG speed (gen est) calculated by the benchmark BEMF Technology (gene ref) of the wind-P&O MPP scheme (gen ref).

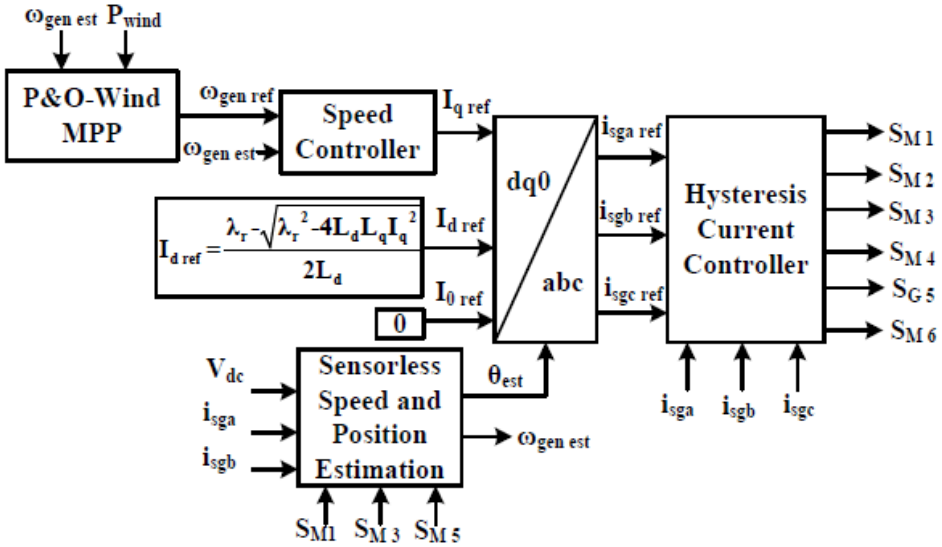

Figure 2.4. Control structure for MVSC control.

D. Bidirectional Converter Controller

Figure.5 shows how to control the bidirectional converter depending on a battery charge status (SOC). The battery reference current is generated using two methods (Ibat ref). Mode 1 is activated when the grid is connected. In Ibat ref, the maximum charging current is used, if the SOC is less than 100 percent. Ibat ref will be null if the SOC is 100% or higher. The battery is stopped charging. Mode 2 is enabled as soon as a grid breakdown occurs. Ibat ref is generated by feeding the DC link voltage mistake to the PI controller. The controller compares the reference battery to the sensed battery current (Ibat). Controller PI compared the reference battery to the sensed current battery (Ibat). Pulse width modulation (PWM) block gets the PI controller Output and generates buck (Sbu)-boot (SB) switching pulses.

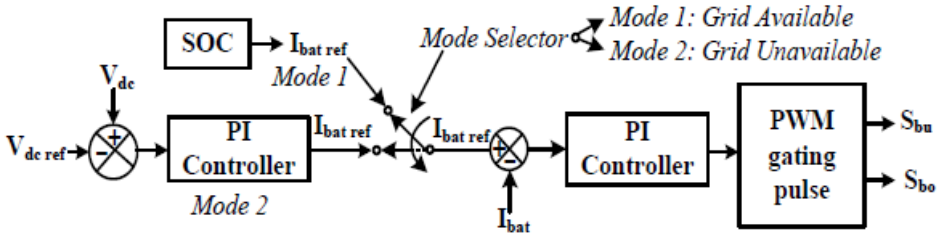

Figure.2.5 Control structure for bidirectional converter.

3. RESULTS

A. Steady State Behaviour of the Micro-grid:

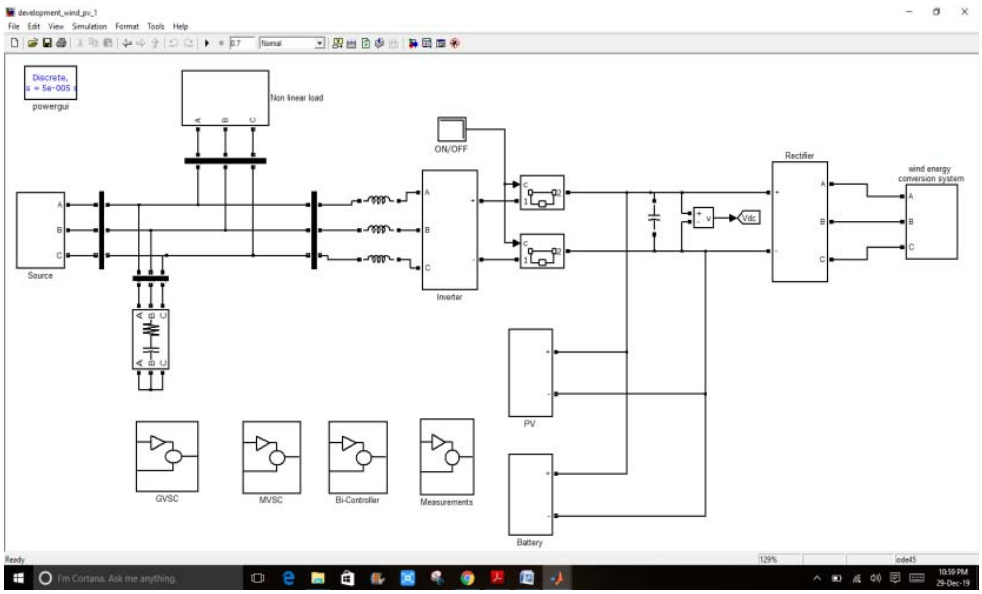

Figure.3.1- Simulation diagram of the micro-grid at steady state condition

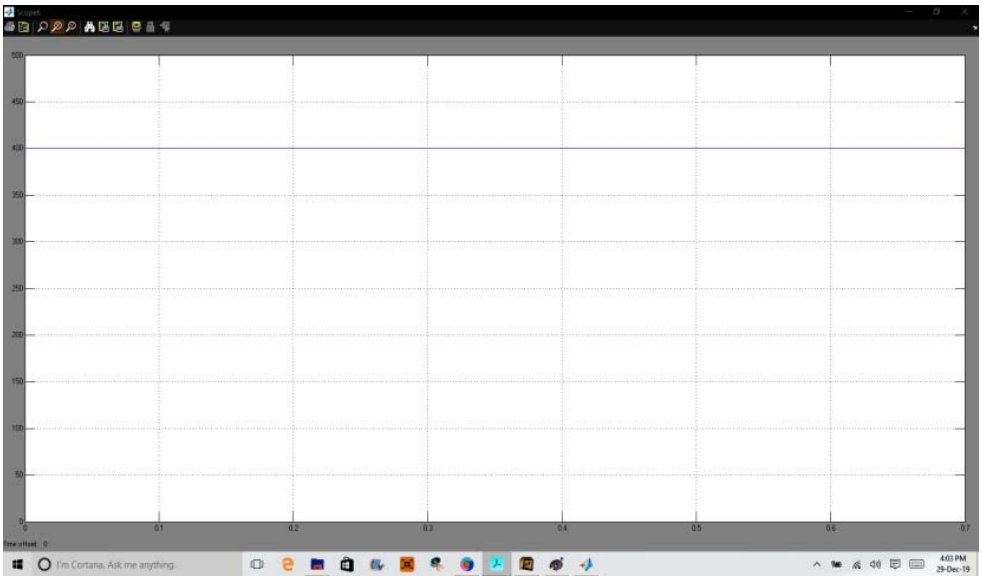

Figure.a- Vdc

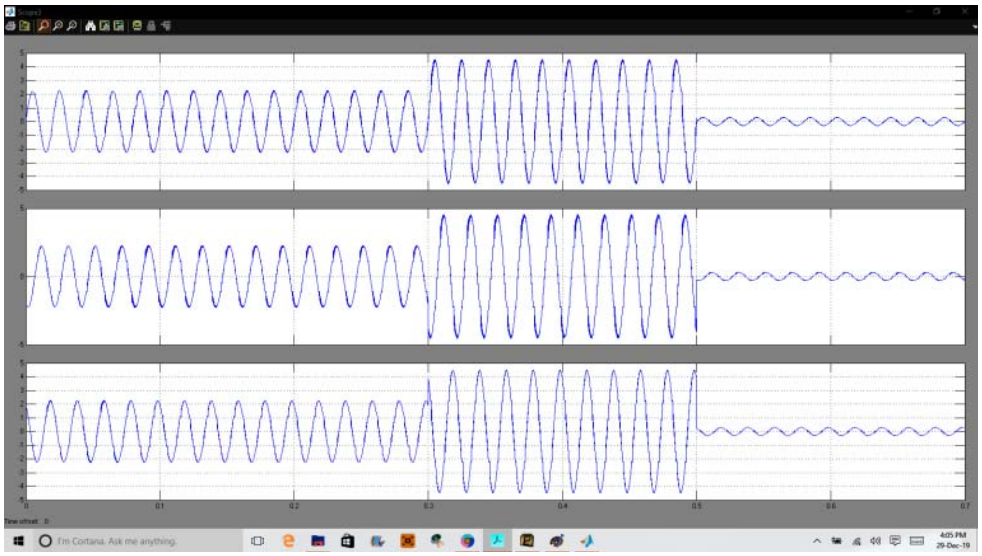

Figure.b- synchronous generator currents(isga, isgb, isgc).

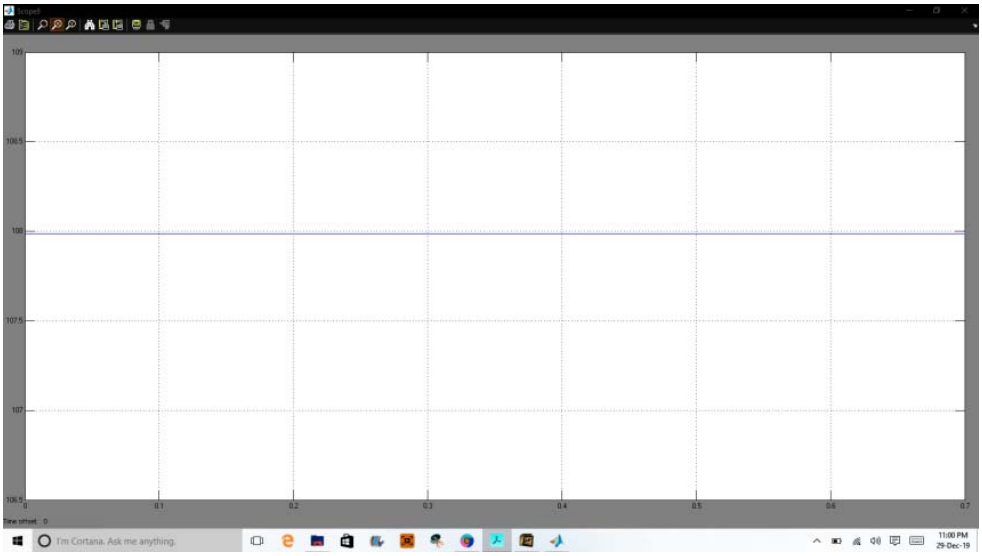

Figure.c- estimated speed (ωgen_est) of SG.

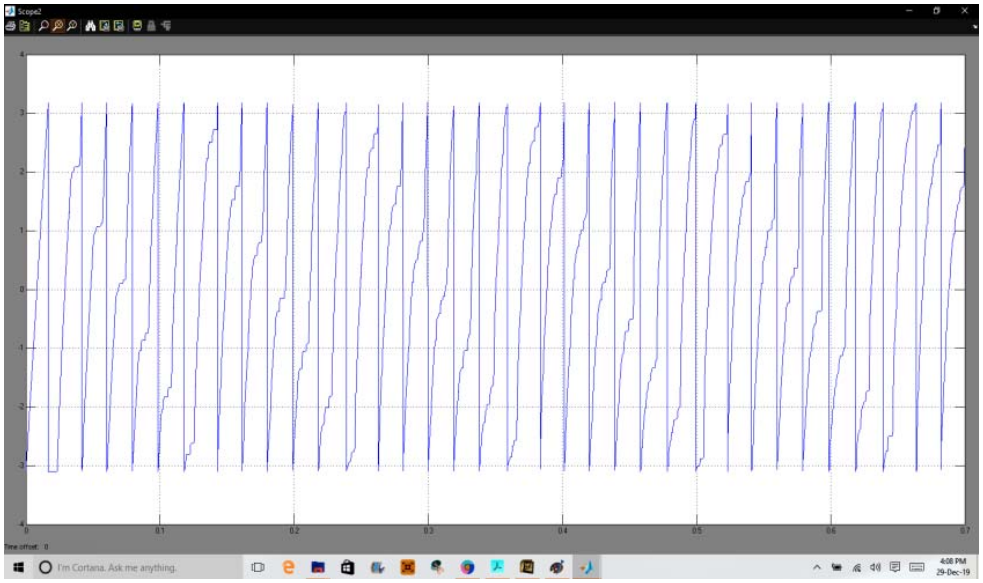

Figure.d- rotor position (θest)

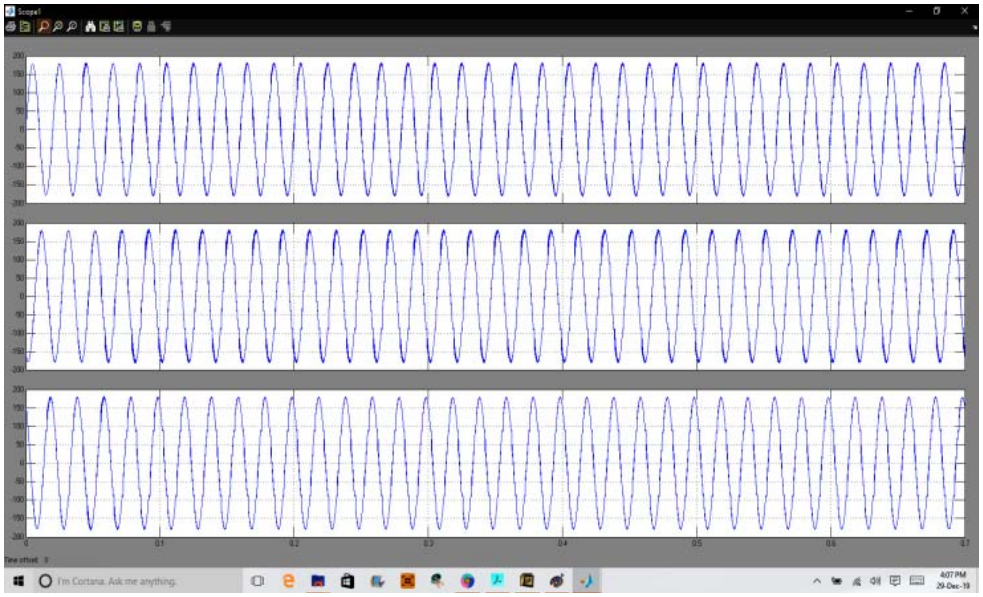

Figure.e- grid voltages

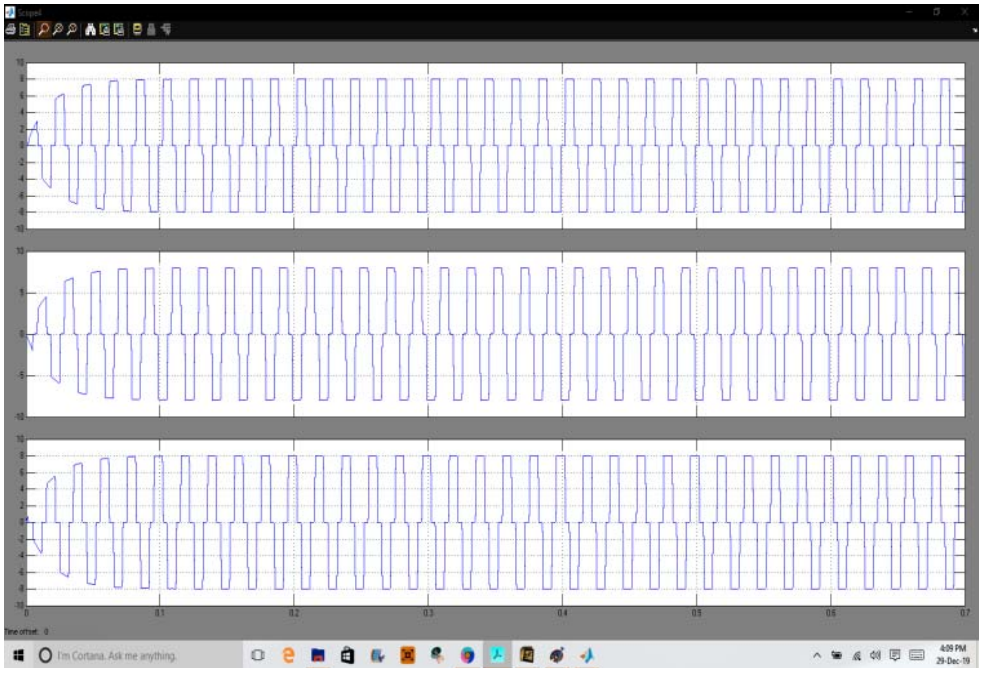

Figure.f- load currents

Figure.g- GVSC currents

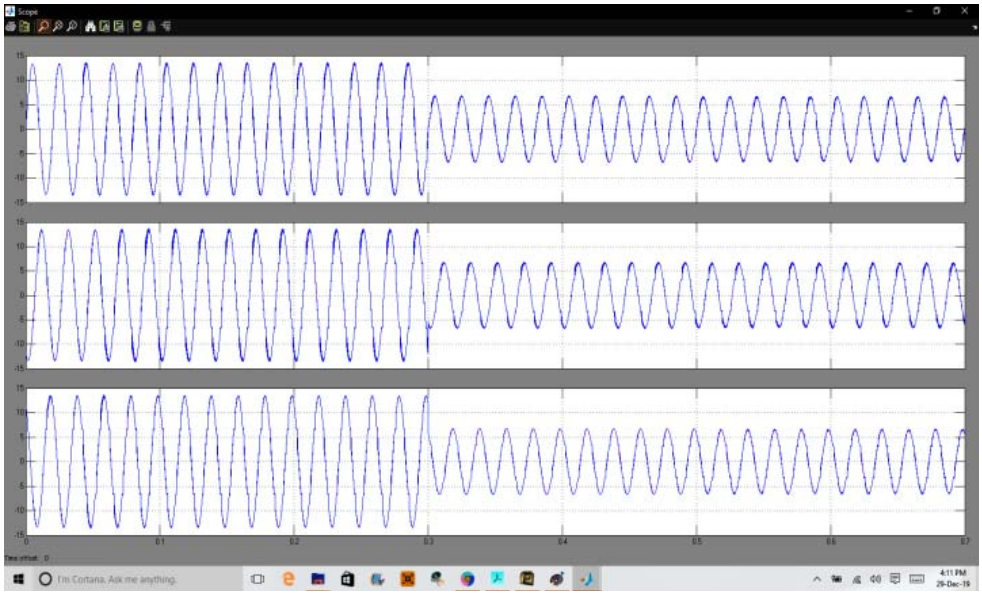

Figure.h- grid currents

The micro-grid performance is shown in Figure.6 in stable condition. The solar and wind power is considered to be in its rated condition and the bidirectional converter maintains the DC connection voltage. The generation from the wind powered SG is low with a low wind speed of 7.2 m/s and 12 m/s, and so the generated currents in magnetic dimensions are. The maximum SG generation is reached when the wind speed reaches cutting speed and can be observed in Figures (a-b). In the conditions mentioned above, the estimated speed (alongside SG), which changes according to the speed of SG and is depicted in Figures, is observed for deceleration and accelerating along with the period of rotor position (alongside) variety (c-d). There are harmonics in the load currents, while the grid currents are balance and sine. The GVSC currents, load currents and phase 'a' grid currents are shown in Figure (e,f,g). The system operates under DSTATCOM mode, when the SG powered by the solar and the wind turbines has nil, and the battery is off. The GVSC provides compensatory currents. The grids current is sinusoidal and undergoes phase reversal and are presented in Figure. (h).

B. Response of Micro-grid under Wind Speed Change:

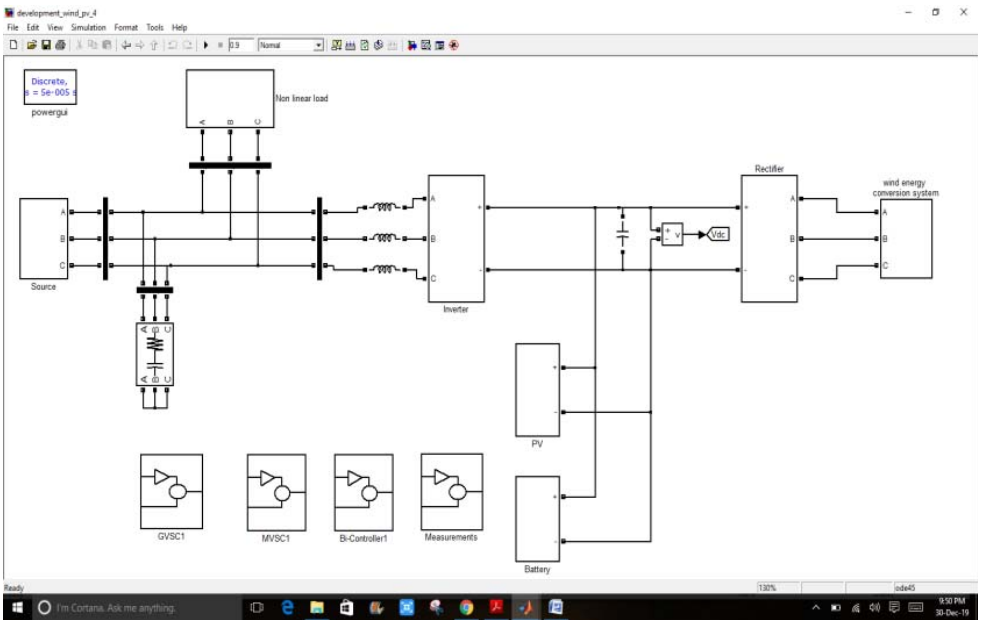

Figure.3.2- Simulation diagram of the micro-grid under wind speed change.

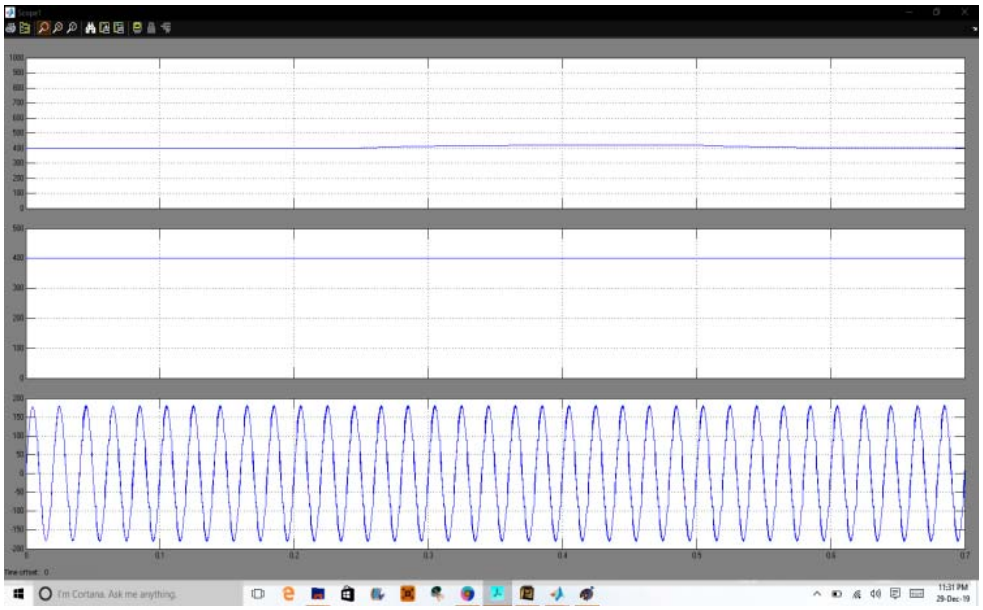

Figure.i- DC link voltage and the AC grid terminal voltage along with the grid voltage of one phase under wind speed rise and fall.

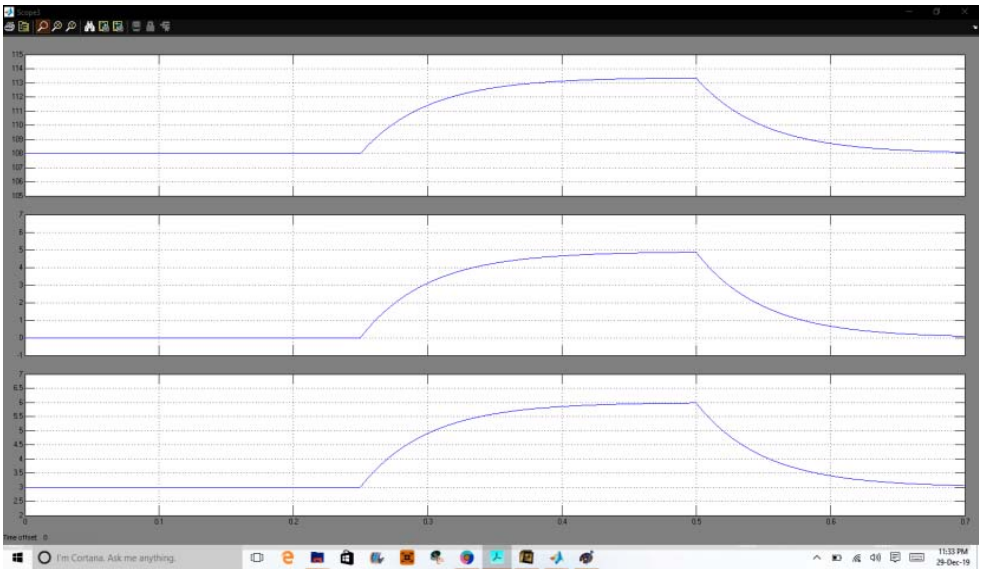

Figure.j- SG estimated speed, direct axis (Id) and quadrature axis (Iq) current.

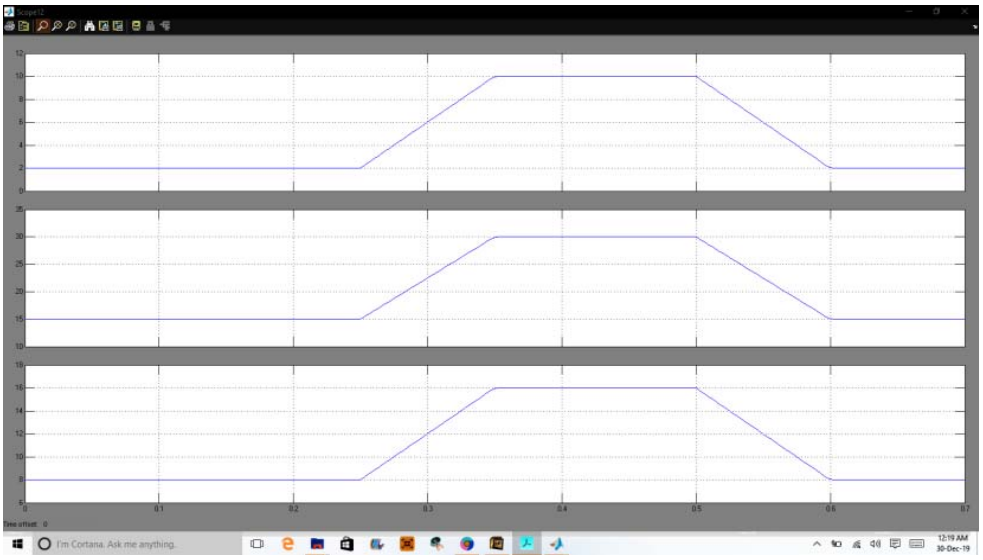

Figure.k- wind feed-forward component (wwff), DC loss component (wloss) and the total weight component (wnet).

The effects of the wind speed must be studied in order to ensure the correct operation of the micro-grid. In Figure. I, when wind speed rises and falls within a wind tunnel, the DC connection tension and a one-stage grid voltage are shown. The bidirectional converter control overcomes the transient voltage of the DC connection and keeps the DC connecting voltage constant. Figure (j) shows SG's estimated speed, direct axis (Id), and quadrature axis currents to show the effect of changes in wind speed (Iq). In Figurers Figure. (k), internal signal changes and the

variation in wind speed and no wind conditions are shown (k). Its size increases with the increase in wind speed as the generation of wind-powered SG increases. The DC loss part (wloss) and the weight component are simultaneously modified (wnet).

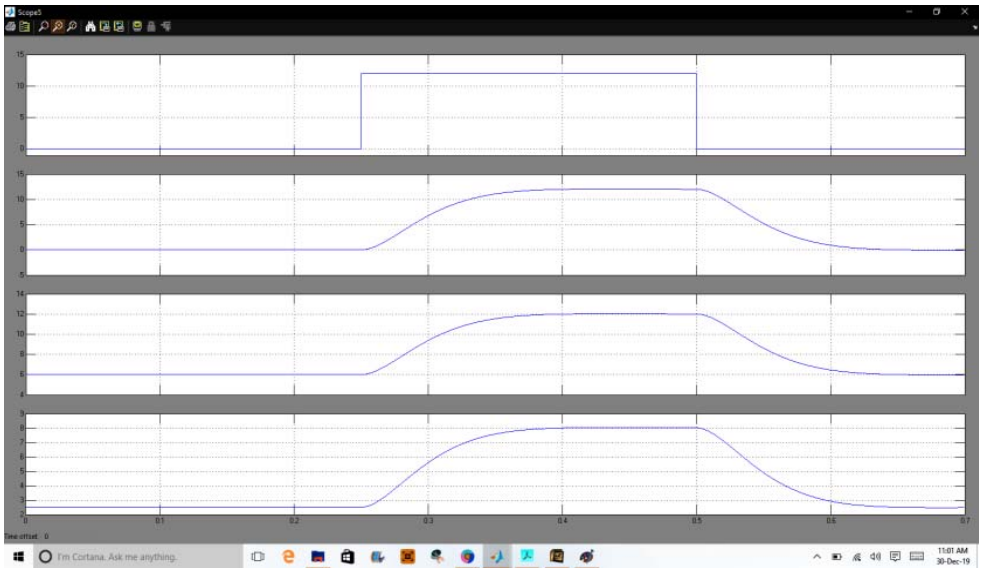

Figure.l- wind feed-forward component (wwff), DC loss component (wloss) and the total weight component (wnet).

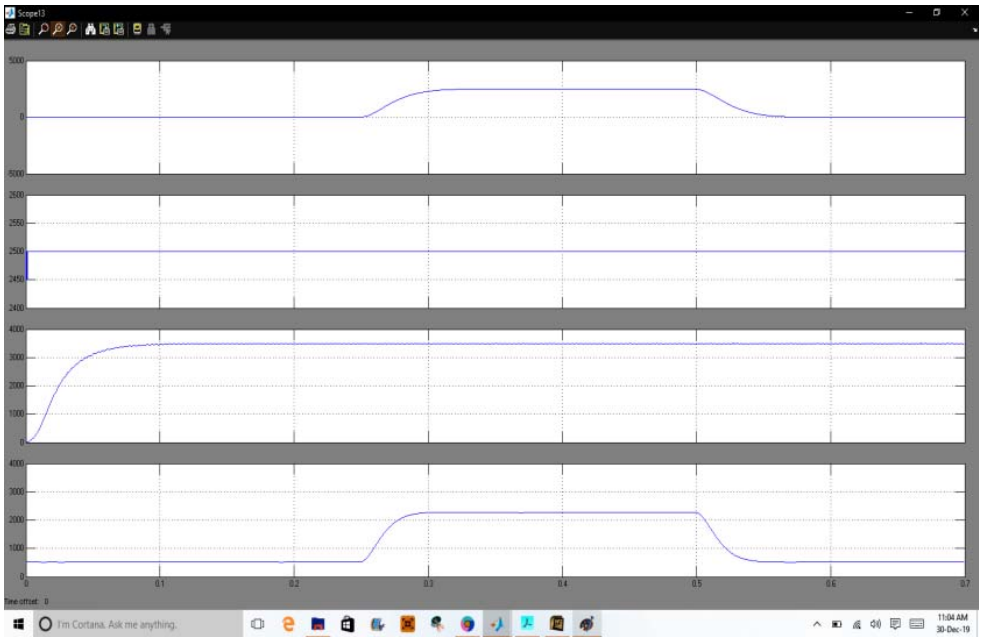

Figure.m- power variations of solar, wind, load and grid

The SG rate increases as the wind speed from 7.2m/s to 12m/s and the Id and Iq components of the SG current increase at the same time. The internal signal changes with

the change of wind speed and no wind conditions are present in Figures. (l). The wind power supply component (wwff) increases in magnitude as wind powered SG generation increases the wind velocity w.r.t. The DC loss (wloss) component and the overall weight component are changed simultaneously (wnet). If the wind velocity is 0, or wind velocity is 0 wwff. If the wind speed is less than that. Figures. (e) show the changes in power of the wind speed system.

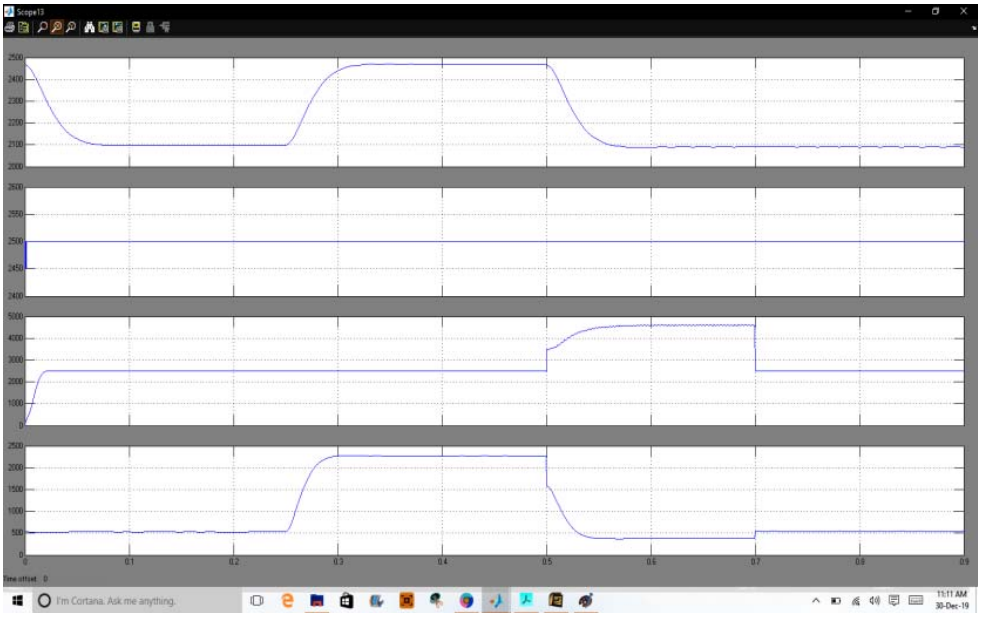

Figure.n- power variations when the load demand is increased and decreased.

In Figure n, you can see how power fluctuates as the load demand increases and decreases. There is a decrease in excess power fed into the grid when renewable energy generation reaches its rated value, and vice versa when the load demand rises.

C. Response of Micro-grid under Solar Insolation Change:

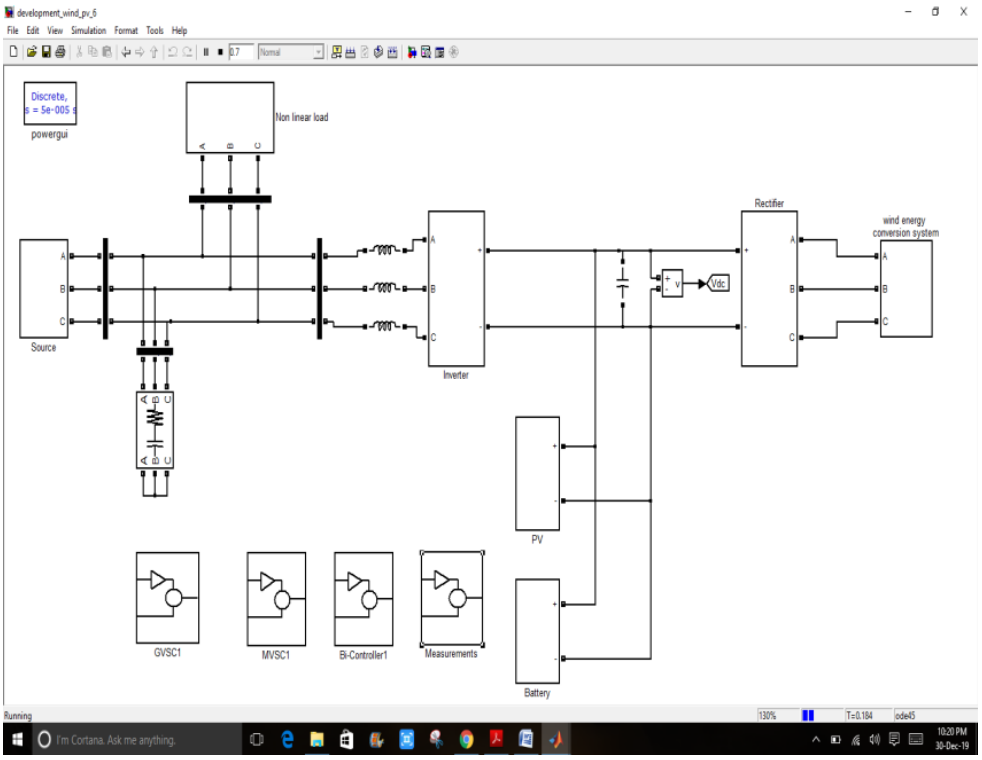

Figure.8- Simulation diagram of the micro-grid under solar insolation variation.

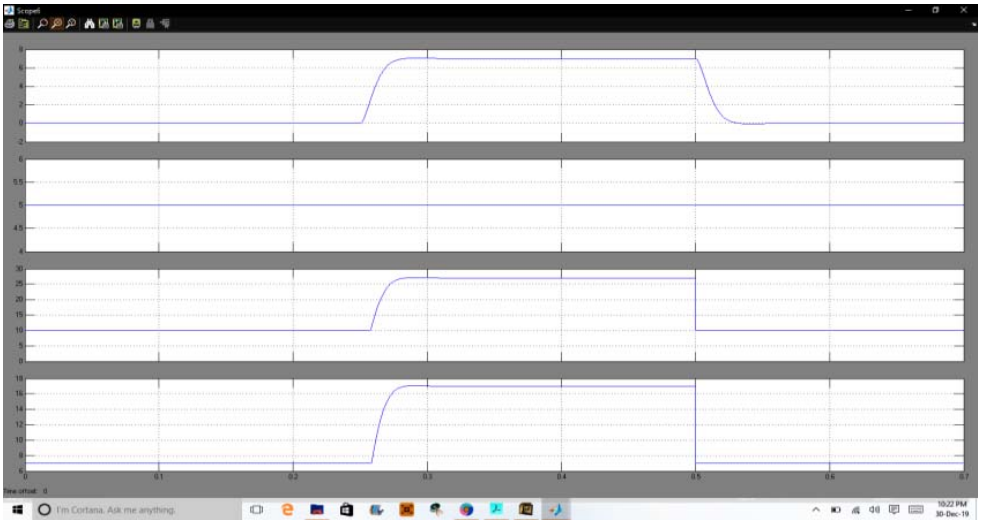

Figure.(o) internal signal variation.

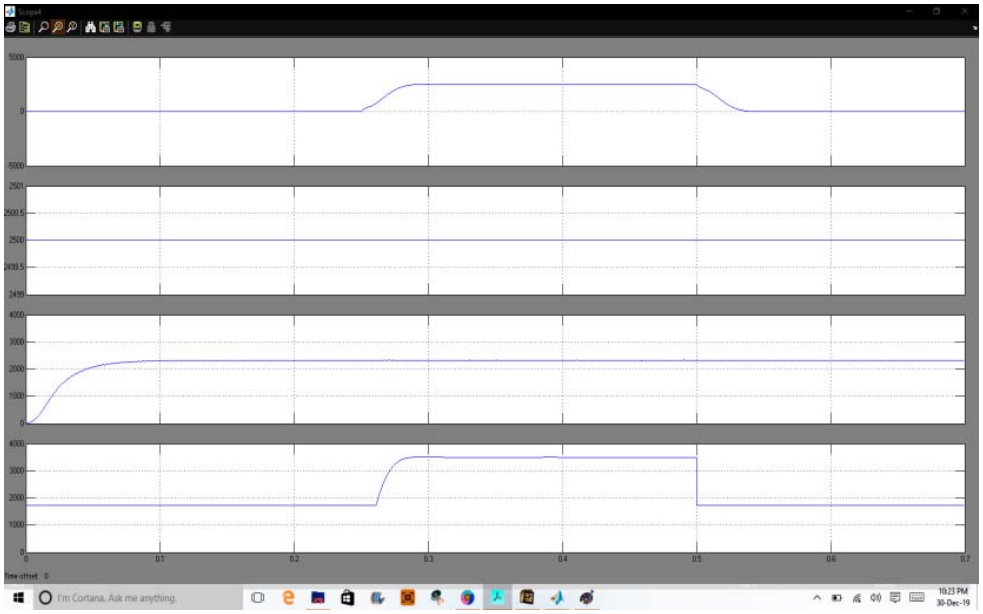

Figure.(p) Power variations.

The intensity of sunlight varies with time and is missing during the night. The performance of the micro-grid as solar insolation changes is shown in Figure 5. In line with changes to solar insolation, PV array current increases and decreases. The two-way converter control eliminates the transient voltage of the DC connector. The AC voltage of the grid is maintained sine quenched. As the Figure shows (o). If the solar insolation increases, the photovoltaic power supply (wpvff) is increased and at zero insolation. The load weight component does not change until wind, BES and grid generation meet the demand for load. Increases in wloss and wnet values can be observed at the same time. Figure (p) Shows how solar, wind, load and grid power vary with changes in the solar insolation. The micro-grid generates enough power to meet the load demand.

4. CONCLUSION

MLMS adaptive control is being used in wind-solar AC micro-grids to improve the power quality. A reduction in harmonics is necessary in the weight of the component and system, as well as in general system performance. The result was achieved by successfully removing the basic load current component with low static mistakes and fast convergence rates. In MATLAB Simulink, the prototype has been tested with wind speed and solar insolation from morning to night and variations in load from the domestic and medium-sized systems.

5. REFERENCES

[1] Y.-M. Cheng, Y.-C. Liu, S.-C. Hung, and C.-S. Cheng, "Multi-input inverter for grid-connected hybrid PV/wind power system," IEEE Trans. Power Electron., vol. 22, no. 3, pp. 1070–1076, May 2007.

[2] S. Yu, L. Zhang, H. H. C. Iu, T. Fernando, and K. P. Wong, "A DSE-based power system frequency restoration strategy for PV-Integrated power systems considering solar irradiance variations," *IEEE Trans. Ind.Informat.*, vol. 13, no. 5, pp. 2511–2518, Oct. 2017.

[3] M. A. Elhadidy "Performance evaluation of hybrid (wind/solar/diesel) power system. Renew Energy" 2002:401–13.

[4] P. Mochi, "Primary Review on MPPT Method and Size of Grid Connected Solar Photovoltaic Inverter," *2018 8thIEEE India International Conference on Power Electronics (IICPE)*, JAIPUR, India, 2018, pp. 1-6.

[5] S. Dasgupta, *et al.*, "A plug and play operational approach for implementation of an autonomous-micro-grid system," in *IEEE Trans. Ind. Informatics*, vol. 8, no. 3, pp. 615-629, Aug. 2012.

[6] K. Sarita *et al*., "Power Enhancement with Grid Stabilization of Renewable Energy-Based Generation System Using UPQC-FLC-EVA Technique," in *IEEE Access*, vol. 8, pp. 207443-207464, 2020, doi: 10.1109/ACCESS.2020.3038313

[7] D. Gallo, R. Langella, A. Testa, J. C. Hernandez, I. Papic, B. Blazic, and J. Meyer, "Case studies on large PV plants: Harmonic distortion, unbalance and their effects," *IEEE Power & Energy Society General Meeting*, 2013.

[8] M. Farhoodnea, A. Mohamed, H. Shareef, and H. Zayandehroodi, "An enhanced method for contribution assessment of utility and customer harmonic distortions in radial and weakly meshed distribution systems," *International Journal of Electrical Power and Energy Systems*, vol. 43, pp. 222-229, 2012.

[9] X. Hou, Y. Sun, J. Lu, X. Zhnag, L. H. Koh, M. Su and J.M.Guerrero, "Distributed hierarchical control of AC micro-grid operating in grid-connected, islanded and their transition modes," IEEE Access, vol. 6, pp. 77388-77401, 2018.

[10] S. Boudoudouh and M. Maaroufi, "Renewable energy sources integration and control in railway micro-grid," IEEE Trans. Ind. Appl., Early Access, 2019.

[11] A. R. Millner, C. Smith, R. Jaddivada and M. Ilic, "Component standards for stable micro-grids," IEEE Trans. Pow. Sys., Early Access, 2018.

[12] A. Radwan and Y. Mohamed, "Grid-connected wind-solar cogeneration using back-to-back voltage source converters," IEEE Trans. Sustain. Energy, Early Access, 2019.

[13] S. Chattopadhyay, M. Mitra, and S. Sengupta, *Electric power quality*. West Bengal, India: Springer, 2011.

[14] S. Haykin, *Adaptive Filter Theory.* Englewood Cliffs, NJ: Prentice- Hall, 1986.

[15] B. Widrow and S. D. Stearns, *Adaptive Signal Processing.* Englewood Cliffs, NJ: Prentice-Hall, 1985.

[16] J. G. Proakis, "Channel identification for high speed digital communications," *IEEE Trans. Automat. Contr.,* vol. AC-19, pp. 916–922, Dec. 1974.

[17] S. Roy and J. J. Shynk, "Analysis of the momentum LMS algorithm," *IEEE Trans. Acoust., Speech, Signal Processing,* vol. 38, Dec. 1990.

[18] R. Sharma, W. A. Sethares and J. A. Bucklew, "Analysis of momentum adaptive filtering algorithms," *IEEE Trans. Signal Proces.*, vol. 46, no. 5, pp. 1430-1434, May 1998.

[19] B. Subudhi and R. Pradhan, "A comparative study on maximum power point tracking techniques for photovoltaic power systems," *IEEE Trans. Sustain. Energy*, vol. 4, no. 1, pp. 89–98, Jan. 2013.

[20] N. Femia, G. Petrone, G. Spagnuolo and M. Vitelli, "Optimization of perturb and observe maximum power point tracking method," *IEEE Trans. Pow. Elect.*, vol. 20, no. 4, pp. 963-973, July 2005.

[21] S. K. Kollimalla and M. K. Mishra, "Variable perturbation size adaptive P&O MPPT algorithm for sudden changes in irradiance," *IEEE Trans. Sustain. Energy*, vol. 5, no. 3, pp. 718-728, July 2014.

[22] J. F. G. Cobben, W. L. Kling and J. M. A. Myrzik, "Power quality aspects of a future micro grid," in *IEEEInternational Conference on Future Power Systems*, 2005